Molecular dynamics simulations of the melting curve of tantalum under pressure

Zhong-Li Liu,[1,2] Ling-Cang Cai,[1] Xiang-Rong Chen,[2,3,*] and Fu-Qian Jing[1,2]
[1]*Laboratory for Shock Wave and Detonation Physics Research, Institute of Fluid Physics, Chinese Academy of Engineering Physics, Mianyang 621900, China*
[2]*Institute of Atomic and Molecular Physics, College of Physical Science and Technology, Sichuan University, Chengdu 610065, China*
[3]*International Centre for Materials Physics, Chinese Academy of Sciences, Shenyang 110016, China*
(Received 7 August 2007; revised manuscript received 26 September 2007; published 7 January 2008)

We have performed coexistence phase molecular dynamics (MD) simulations to investigate the melting curve of tantalum over a wide range of pressures. To ensure faithful MD simulations, three types of potentials, including the extended Finnis-Sinclair (EFS) potential, the long-range empirical potential (LREP), and the force-matching (FM) potential, are fully tested. Through a series of tests, such as equation of states, thermal expansion, and other thermodynamic properties for liquid Ta, we have found that the EFS potential is the reliable potential for simulating both solid and liquid Ta. The EFS potential can also produce a satisfying melting curve, consistent well with both experiments of ambient pressure and shock melting at high pressure. However, the other two melting curves from the LREP and the FM potential have not so satisfying agreement with shocking melting at high pressure. Hence we recommend that the EFS should be the reliable potential for simulating melting properties of Ta as well as other properties of solid and liquid Ta.

DOI: 10.1103/PhysRevB.77.024103 PACS number(s): 64.70.D-, 68.18.Jk, 71.20.Be, 71.15.Pd

I. INTRODUCTION

Melting properties are of fundamental importance for understanding the equilibrium properties of both solid and liquid phases of materials. Scientific investigations on melting properties of metals have been extensively conducted experimentally[1–7] and theoretically,[8–15] particularly for transition metals, such as Ta, Mo, W, and so on, because of their enormous discrepancies in melting curves between laser-heated diamond-anvil cell[4–7] (DAC) and shock wave[2,3] (SW) methods. As for Ta (as well as Mo and W), several thousand degrees of discrepancies exist in extrapolating from DAC pressures of about 100 GPa (Refs. 4–7) to SW pressure of 300 GPa,[2] and the high pressure melting curve of Ta still remains inconclusive up to now.[14]

Bulk Ta belongs to body-centered cubic (bcc) structure at ambient conditions, however, a shock-induced (45 GPa) β (bcc) to ω (hexagonal) displacive transformation was observed by Hsiung and Lassila.[16,17] While other shock experiments[18–20] and theoretical results[8,21,22] indicated that bcc phase remains stable under pressure up to 500 GPa. The DAC experiment[23] demonstrated that the bcc phase continued to be stable up to 174 GPa. In this work, we have also performed first-principles calculations and found no phase transition from bcc phase to hexagonal phase, as will be described below in detail.

As for the melting of Ta, theoretical results are now inadequate to explain the extreme discrepancies in extrapolating the DAC data to the SW data. Moriarty *et al.*[8] employed the model generalized pseudopotential theory (MGPT) and obtained a melting curve that was in fundamental agreement with the SW data but was several thousand degrees higher than the extrapolated DAC data. Strachan *et al.*[11] calculated the melting curve of Ta using classical molecular dynamics (CMD) with embedded atom model (EAM), their obtained results are close to those of Moriarty *et al.* below 100 GPa but not having the similar trend with those of Moriarty *et al.* above 100 GPa. Most recently, Taioli *et al.*[15] calculated the melting curve of Ta from first-principles calculations. Their results were consistent with the SW data but also diverged from DAC data below 100 GPa and are several thousand degrees higher than the extrapolated DAC data at about 300 GPa. Results from the empirical melting models (including Lindemann law, vacancy-model, and dislocation melting model) mainly tend to support the shock results. The dislocation melting curve of Verma *et al.*[12] and Lindemann melting curve of Wang *et al.*[24] both overestimate the melting curve, while Lindemann melting curve of Verma *et al.*[12] accords with shock melting and vacancy melting curve of Errandonea *et al.*[25] is in accordance with the DAC data.

It remains challenging to accurately determine equilibrium melting point of crystals in theory. The most commonly used theoretical methods are solid-liquid coexistence (two-phase) approach[26] and free energy approach.[27] In solid-liquid coexistence approach, the superheating effect can be eliminated by simulating a coexistence system with a solid-liquid interface.[26] Successful application of this method has been reported on a wide range of materials such as Lannard-Jonesium,[28] LiH,[29] MgO and NaCl,[30] fcc and hcp metals,[9] GaN,[31] Fe,[32] and so on. However, a large number of atoms (usually more than 1000 atoms) are necessary for this method to obtain accurate enough results, thus it is very computationally expensive to perform simulations using *ab initio* molecular dynamics (AIMD) with coexistence approach. The free energy approach is based on the equality of the Gibbs free energy of the solid and the liquid at the equilibrium melting point,[27] and a relatively smaller number of atoms (less than 200 atoms) are required to achieve accurate results. We here report a detailed molecular dynamics investigation on the high-pressure melting line of Ta to further understand the melting properties of Ta with coexistence approach.

II. METHODOLOGY

A. Potential functions

For molecular dynamics (MD) simulations of melting of Ta, we adopted three types of potential forms to compare which one is appropriate to simulate the melting properties of Ta at high pressures and high temperatures. The first type is the recently developed extended Finnis-Sinclair potential (EFS),[33] in which the total potential energy has the following form:

$$U_{\mathrm{tot}} = \frac{1}{2}\sum_{ij} V(r_{ij}) - \sum_{i} f(\rho_i). \tag{1}$$

The first term in Eq. (1) is the conventional central pair-potential, in which $V(\mathrm{r})$ is expressed by

$$V(r) = \begin{cases} (r-c)^2(c_0 + c_1 r + c_2 r^2 + c_3 r^3 + c_4 r^4), & r \leqslant c, \\ 0, & r > c, \end{cases} \tag{2}$$

where c is a cutoff parameter assumed to lie between the second and the third neighbor atoms. c_0, c_1, c_2, c_3, and c_4 are the potential parameters. The second term in Eq. (1) is the n-body term. The embedding function f can be expressed by

$$f(\rho_i) = \sqrt{\rho_i}, \tag{3}$$

where the host electronic density ρ_i can be written as the sum of the electronic density functions $\phi(r_{ij})$ of the individual atoms i

$$\rho_i = \sum_{j \neq i} A^2 \phi(r_{ij}), \tag{4}$$

The electronic density function is expressed by

$$\phi(r) = \begin{cases} (r-d)^2 + B^2(r-d)^4, & r \leqslant d, \\ 0, & r > d, \end{cases} \tag{5}$$

where d is also the cutoff parameter to be assumed to lie between the second and the third neighbor atoms. All the parameters are fitted well to reproduce lattice constants, cohesive energies, elastic constants, and vacancy formation energies of Ta. The fitted parameters for Ta are[33] c_0=30.91155 eV/Å^2, c_1=−26.57902 eV/Å^3, c_2=6.651629 eV/Å^4, c_3=0.0070699 eV/Å^5, c_4=−0.128597 eV/Å^6, c=3.77 Å, A=2.702029 eV/Å, d=4.15 Å, and B=0.

The second type of potential is the most recently developed long-range empirical potential (LREP),[34] in which the total potential energy of E_{i} of an atom i is expressed as

$$E_i = \frac{1}{2}\sum_{j \neq i} \phi(r_{ij}) - \sqrt{\sum_{j} \varphi(r_{ij})}. \tag{6}$$

In Eq. (6), the first and the second term are the repulsive pair term and n-body term, respectively. $\phi(r_{ij})$ is expressed by

$$\phi(r_{ij}) = \begin{cases} (r_{ij} - r_{c1})^m (x_0 + x_1 r_{ij} + x_2 r_{ij}^2 + x_3 r_{ij}^3 + x_4 r_{ij}^4), & r_{ij} \leqslant r_{c1}, \\ 0, & r_{ij} > r_{c1}, \end{cases} \tag{7}$$

where r_{c1} is a cutoff radius and x_0, x_1, x_2, x_3, and x_4 are the potential parameters. In the LREP model, $\varphi(r_{ij})$ is expressed as

$$\varphi(r_{ij}) = \begin{cases} \alpha(r_{ij} - r_{c2})^n \exp\left[-\beta\left(\frac{r_{ij}}{r_0} - 1\right)\right], & r_{ij} \leqslant r_{c2}, \\ 0, & r_{ij} > r_{c2}, \end{cases} \tag{8}$$

where r_{c2} is also a cutoff radius and r_0 is the first-neighbor distance. α and β are two potential parameters. The fitted parameters for Ta are[34] m=4, n=6, r_{c1}=5.079 Å, r_{c2}=6.700 Å, x_0=6.618 eV/Å^4, x_1=−8.748 eV/Å^5, x_2=4.370 eV/Å^6, x_3=−0.9714 eV/Å^7, x_4=0.08081 eV/Å^8, r_0=2.8579 Å, α=0.0031530 eV^2/Å^6, and β=0.1175.

The third type of potential for Ta is the embedded-atom-method (EAM) potential developed with the force-matching (FM) method[35] by Li *et al.*[36] The functional form of the EAM potentials is given by

$$E_{\mathrm{tot}} = \frac{1}{2}\sum_{i \neq j} V(r_{ij}) + \sum_{i} F(\rho_i), \tag{9}$$

$$\rho_i = \sum_{j} \phi(r_{ij}). \tag{10}$$

where E_{tot} is the total energy, $V(r_{ij})$ the pair potential, and $F(\rho)$ the embedding function. $\phi(r_{ij})$ is the electron density contribution from atom j to atom i. The total electron density ρ_i at an atom position i is calculated via the linear superposition of electron density contributions from neighboring atoms. The FM potential of Ta has been fitted to a variety of experimental data including elastic constants, lattice constant, cohesive energy, unrelaxed vacancy formation energy, and density-functional theory data for various structures including clusters, surfaces, interstitials, vacancies, liquids, and stacking faults. The numerical form of FM potential of Ta was created as a file for using conveniently.[37]

B. Molecular dynamics simulations

1. Phase of bulk Ta

We first made first-principles calculations to make clear the phase of Ta. To obtain the energy as a function of atomic volume and the enthalpy as a function of pressure, we apply the full-potential (FP) linear muffin-tin orbital (LMTO) method with exchange-correlation functional of the generalized gradient approximation (GGA) proposed by Perdew, Burke, and Ernzerhof.[38] The present results were obtained by using the LMTART code.[39] All relativistic effects were taken into account except the spin-orbit interaction for the valence electrons, where the scalar relativistic equations were solved. The crystal space was partitioned into the nonoverlapping

TABLE I. Comparison between *ab initio* and experimental EOS parameters: V_0, B_0, and B_0' are volume, bulk modulus, and its pressure derivative at zero pressure, respectively. $\Delta V_0=(V_0-V_{0\,\mathrm{expt}})/V_{0\,\mathrm{expt}}$.

	V_0 (Å^3)	ΔV_0 (%)	B_0 (GPa)	B_0'
This work	18.245	1.16	193	3.88
Expt. (Ref. 41)	18.035		194	3.52

muffin-tin spheres surrounding every atom and the remaining interstitial region. The basis set was comprised of augmented linearized muffin-tin orbitals.[40] The muffin-tin (MT) sphere radius R_{MT} was chosen as 3.161 a.u. for the Ta atom. Inside the MT spheres, the basis functions, charge density, and potential were expanded in symmetry adapted spherical harmonic functions together with a radial function. We used Fourier series in the interstitial regions. The maximum angular momentum component for the spherical-harmonic expansion was $l_{\max}=6$. The K-space integrations were performed by using $12\times12\times12$ to obtain good convergence of energy. The calculated energies were fitted to the fourth-order Birch-Murnaghan equation

$$P=3B_0f_E(1+2f_E)^{5/2}\left\{1+\frac{3}{2}(B'-4)f_E+\frac{3}{2}\left[B_0B''+(B'-4)(B'-3)+\frac{35}{9}\right]f_E^2\right\}, \quad (11)$$

where $B_0=-V_0\frac{d^2E}{dV^2}$, $f_E=[(V_0/V)^{2/3}-1]/2$, $B'=\frac{\partial B}{\partial P}$, and $B''=\frac{-1}{B_0}\left[(3-B')(4-B')+\frac{35}{9}\right]$. The pressure P and the energy E were correlated through the following thermodynamic relationship:

$$P=-\frac{dE}{dV}. \quad (12)$$

The fitted results are compared with experimental values[41] in Table I. The obtained equilibrium volume V_0 and zero-pressure bulk modulus both accord well with experiment.[41]

The calculated E-V and H-P data are also shown in Fig. 1. It is noted that bcc phase is more stable than hexagonal phase and the transition from bcc to hexagonal can not take place according to the curve of enthalpy. This conclusion is also supported by the shock experiments[18–20] and other theoretical results.[8,21,22] Therefore, in present work, we treat bcc phase as the unique phase in our molecular dynamics simulations, and we believe that melting of Ta takes place from bcc phase within the whole range of pressure of interest.

2. Details of MD simulations

The MD simulation supercell consisted of $8\times8\times21$ conventional unit cell (2688 Ta atoms) in bcc structure and the initial size of the simulation box was $26.4208\times26.4208\times69.3546$ Å^3. Three-dimensional periodic boundary conditions were applied. From our tests on size dependence of melting point, we know 2688 atoms are sufficient for simulating the melting curve of Ta at all pressures of interest.

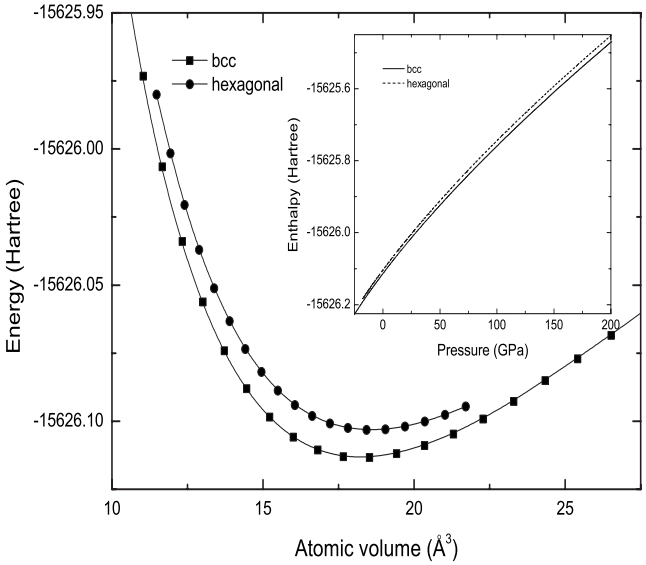

FIG. 1. Calculated energy as a function of atomic volume, indicating the bcc phase is more stable than hexagonal phase. In the inset, the enthalpy as a function of pressure is presented. No phase transition from bcc to hexagonal was found.

To construct initial configuration of solid-liquid coexistence, we froze the outer two parts (1792 atoms) of the box along the z axis, then heated one third number of the atoms (896 atoms) in the center of the box along the z axis up to 6000 K (far beyond melting point) in NVE ensemble to equilibrium after 30 ps. As a result, a box that contained two solid and one liquid phase with two interfaces was built. This box was used as the initial configuration for further simulations. All the simulations are performed using the DL_POLY2.17 program.[42]

The Berendsen isothermal-isobaric (NPT) ensemble[43] were used to achieve constant temperature and pressure. A cutoff distance of 8 Å was applied to the van der Waals interactions and the electrostatic interaction was calculated using the smooth particle mesh Ewald algorithm.[44] The relaxation times for the thermostat and barstat were 1.0 and 3.0 ps, respectively. The time step for trajectory integration was 3.0 fs. The total simulation time steps were 10000, which was tested to be sufficient for current coexistence phase simulations. The first 6000 steps were used for equilibrium, and the last 4000 steps for statistical average of properties such as volumes and energies.

C. Equilibrium melting point

The built initial configuration with two interfaces are shown in Fig. 2(a), in which we plot the average number density in slices of the cell taken parallel to the boundaries between solid and liquid. The solid part is identified by periodic oscillations of the density, while the density of liquid part fluctuates randomly with much smaller amplitude.

At a fixed pressure, when system temperature is below melting point, the interfaces will move towards the liquid part, i.e., the liquid part will be continuously crystallized [Fig. 2(b)]. While, when system temperature is above melt-

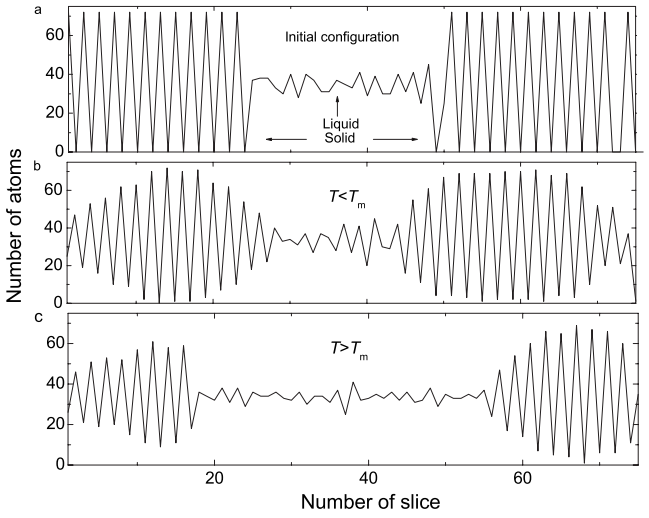

FIG. 2. Density profile for the coexistence configuration of two solid phases and one liquid phase. The solid phase is identified by periodic oscillations of the density, while the density of the liquid phase fluctuates with much smaller amplitude. (a) The initial configuration, (b) The moving of interfaces towards liquid part when $T<T_m$, (c) The moving of interfaces towards solid parts when $T>T_m$. The simulation box contained 2688 atoms and the slice width was 0.925 Å.

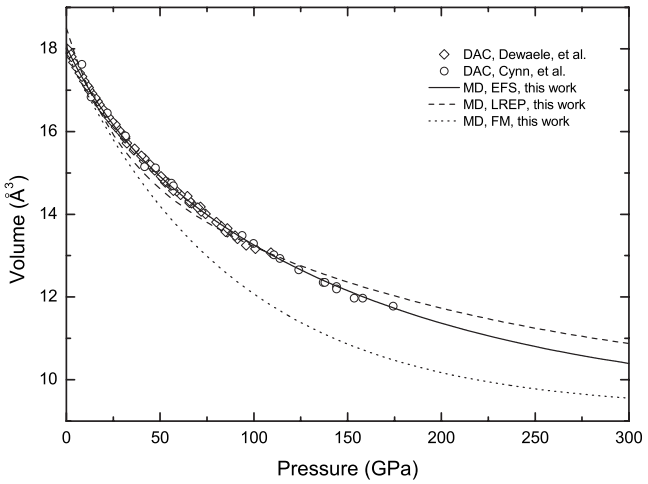

FIG. 3. Comparison of the calculated 300 K isotherms for the three types of potentials with DAC experiments. The results show that the isotherm obtained from the extended Finnis-Sinclair (EFS) potential have the best agreement with DAC experiments (Refs. 23 and 41) in all three potentials.

ing point, the interfaces will move towards the solid parts, i.e., the solid parts will be progressively melted [Fig. 2(c)]. So we can judge the temperature is either below or above melting point at a fixed pressure by monitoring the moving direction of the interfaces from the average number density in slices, and then narrow the range of melting temperature by a certain amount of trials and errors at this pressure. Then we can obtain the whole melting curve within the whole range of pressure of interest by repeating the above steps.

III. RESULTS AND DISCUSSIONS

A. Equation of states and thermal expansion

To assess on the qualities of the three types of potentials, we have performed MD simulations at pressures up to 300 GPa and at temperatures up to 3000 K. No phase transitions were found, as accords with the *ab initio* calculations of ours and others,[8,21,22] and the shock experiment.[18–20] The calculated 300 K isotherms by using the three types of potentials are plotted in Fig. 3, in which we also compare the results obtained from the three types of potentials with DAC experiments.[23,41] Obviously, the extended Finnis-Sinclair (EFS) potential is in best agreement with experiments in the whole pressure range where the DAC data exist. At ambient conditions, the obtained equilibrium volume (18.041 Å^3) from EFS is only 0.033% larger than experimental value 18.035 Å^3.[41] The result of long-range empirical potential (LREP) is consistent well with DAC experiments below 150 GPa, but it deviates from DAC above 150 GPa, while the result from the force-matching potential deviates greatly from DAC at all pressures, as is probably due to the fact that FM potential is obtained mainly by fitting forces data which are less reliable than fitting energies.[45]

Thermal expansion of a solid is a direct consequence of the anharmonicity of lattice vibrations and is a direct manifestation of the anharmonic nature of the interatomic forces, and it thus can provide a convenient measure of the anharmonic parameters for a crystal. For the calculations of melting properties, the response of a potential to temperature is crucial to simulate the anharmonic nature of the interatomic forces in a solid. The assessment of a potential response to temperature can be made by comparing the thermal expansion properties from the potential with those from experiments. We have calculated the volumes of Ta at pressure of 1 bar and at temperatures from 300 to 3000 K. The lattice constant as a function of temperature and linear coefficient of thermal expansion were calculated from these volumes, and the comparison with experiment[46] is shown in Fig. 4. The linear coefficient of thermal expansion was obtained using $(a\text{-}a_0)/a_0$, where a_0 is the lattice constant at $T=300$ K. It can be seen clearly that the result of the EFS potential is also comparatively consistent with experiment, i.e., the EFS potential can mainly reflect the anharmonic nature of interatomic force in Ta. However, the other two types, especially LREP, have the worse reflection of anharmonicity at high temperatures.

B. Properties of liquid Ta

The capability of a potential for description of liquid properties is another standard to assess its suitability for simulating melting properties. So, we have also calculated the volumes of liquid Ta at various temperatures and at a pressure of 0.2 GPa using the three types of potentials. From these volumes we obtained the densities of liquid Ta as a function of temperature, as are compared with experiment[47] in Fig. 5. We note that the EFS potential is also reliable to

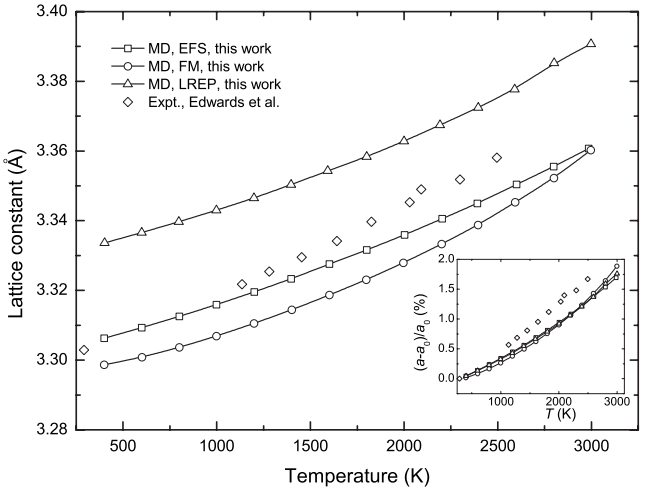

FIG. 4. Lattice constant and linear coefficient of thermal expansion (the inset) of Ta as a function of temperature from the three types of potentials in comparison with experiments (Ref. 46). The EFS potential is most consistent with experiment among the three types.

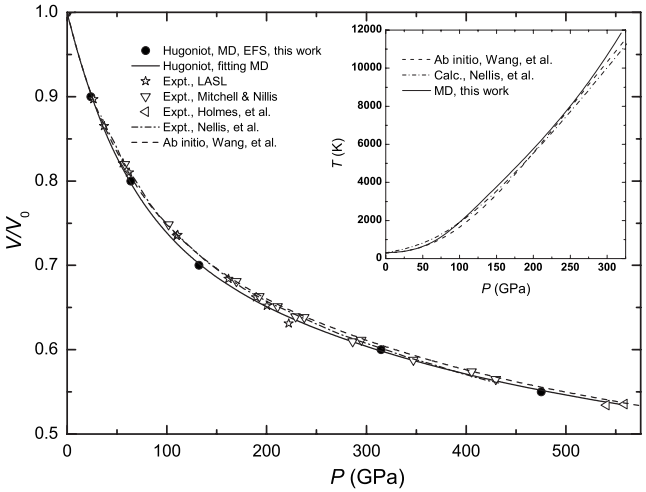

FIG. 6. The volume-pressure and temperature-pressure (the inset) relations on Hugoniot are obtained from molecular dynamics using EFS potential. The agreement of our result with experiments (Refs. 19, 20, and 48) and *ab initio* calculations (Ref. 49) is excellent.

describe liquid Ta as solid Ta. However, the LREP and FM potentials, in particular FM potential, are not in good agreement with experiment. From the above assessments for the three types of potentials of solid and liquid Ta, we believe that the EFS potential has the best quality to describe both solid and liquid phase of Ta in all three potentials.

C. Hugoniot properties

From EFS potential, we obtained Hugoniot curve according to the Rankine-Hugoniot formula

$$p_H(V_0 - V_H) = 2(E_H - E_0), \tag{13}$$

where E_H is the molar internal energy along the Hugoniot and E_0 and V_0 are the molar internal energy and volume at zero pressure and room temperature, respectively. The pressure-volume and temperature-pressure relations along the Hugoniot are obtained according to Eq. (13). For a given volume, we adjusted temperature and obtained pressure and energy from molecular dynamics until the Rankine-Hugoniot relation was satisfied. The obtained Hugoniot of pressure-volume and temperature-pressure are presented in Fig. 6. Together with experiments[18–20,48] and *ab initio* calculations.[49] The Hugoniot from EFS potential is in excellent agreement with experiments and *ab initio* calculations.

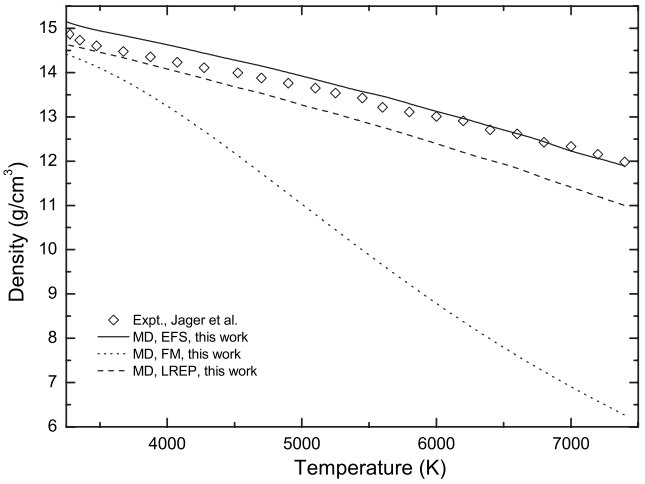

FIG. 5. Density of liquid Ta as a function of temperature at a pressure of 0.2 GPa. The EFS potential is in best agreement with experiment (Ref. 47).

D. Sound velocity in shocked liquid Ta

To further test the quality of the EFS potential, we obtained the sound velocity of shocked liquid Ta from the EFS potential using the molecular dynamics simulations. The Grüneisen parameter is a most important parameter, particularly for reduction of shock data, and is defined by

$$\gamma = V\left(\frac{\partial p}{\partial E}\right)_V = \frac{\alpha K_T V}{C_V}, \tag{14}$$

where E, α, K_T, and C_V are the internal energy, the coefficient of thermal expansion, isothermal bulk modulus, and constant volume specific heat, respectively. From the Grüneisen parameter the bulk velocity of shocked Ta of liquid can be obtained via

$$C^2 = -V^2\frac{dp}{dV}\left[1 - \left(\frac{\gamma}{V}\right)V_0\frac{\eta}{2}\right] + V^2\left(\frac{\gamma}{V}\right)\frac{p}{2}, \tag{15}$$

where $\eta = 1 - V/V_0$, dp/dV is the derivative of p with respective to V along the Hugoniot, and V_0, V, and p are the volume at ambient conditions, the volume after shocked, and shock pressure, respectively.

The calculated Grüneisen parameters and the sound velocities from the EFS potential of liquid Ta are listed in Table

TABLE II. The calculated Grüneisen parameters and the sound velocities of liquid Ta at various pressures, compared with shock experiment. The pressures are in GPa and the sound velocities are in km/s.

Pressure	325	340	350	390	435
γ	1.15	1.12	1.11	1.05	1.02
C (cal.)	6.627	6.728	6.782	7.021	7.254
C [expt. (Ref. 2)]	6.440	6.542	6.604	6.848	7.128

II, and the sound velocities are also presented in Fig. 7, compared with shock experiment[2] and *ab initio* results.[50] The agreement with experiment and *ab initio* results is reasonably good. So we believe the EFS potential is reliable to simulation high pressure and high temperature properties of both solid and liquid tantalum.

E. Melting properties

Using the coexistence phase method described above, we calculated the melting curves with the three types of potentials and the results are presented in Fig. 8, compared with experimental and theoretical results. The melting temperatures from EFS potential at various pressures are shown in Table III. The calculated melting temperature from EFS potential at ambient pressure is 3225±25 K, which is in excellent agreement with experimental results that range from 3213 to 3273 K.[4,51] At high pressure of 307 GPa, our melting point is 8550±50 K, consistent with shock melting temperature of 8500±1500 K (Ref. 2) (superheated to some extent) at about 300 GPa and close to *ab initio* value of 9783±85 K (Ref. 15) at 307 GPa. The calculated three melting curves are all in good agreement with DAC experiments in the very low pressure region. While, in the pressure range of around 10–100 GPa, our three melting curves all diverge from DAC values with increasing pressure as well as other theoretical results.[8,11,12,15,24,25] And our results of EFS potential agree well with *ab initio* results of Taioli *et al.*[15] below 100 GPa, but above 100 GPa, the results are lower than those of Taioli *et al.* However, the other two curves of LREP and FM potentials have not the satisfying agreement with shocking melting at high pressure, as is because their tested properties described above are in worse agreements with experiments.

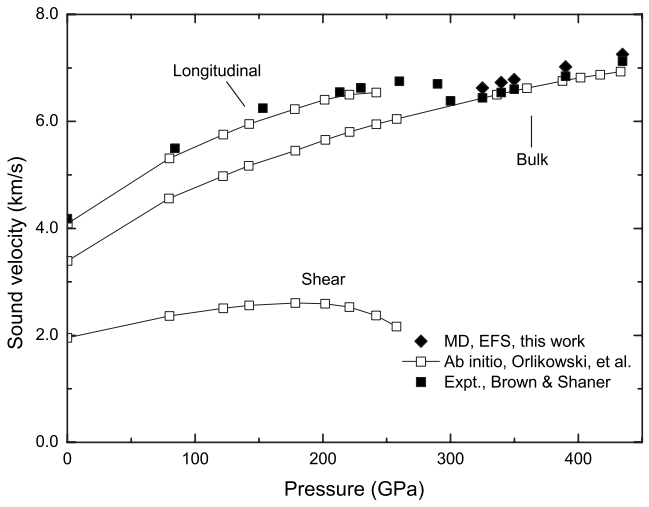

FIG. 7. The obtained sound velocities of shocked liquid Ta from the EFS potential, compared with shock experiment (Ref. 2) and *ab initio* results (Ref. 50).

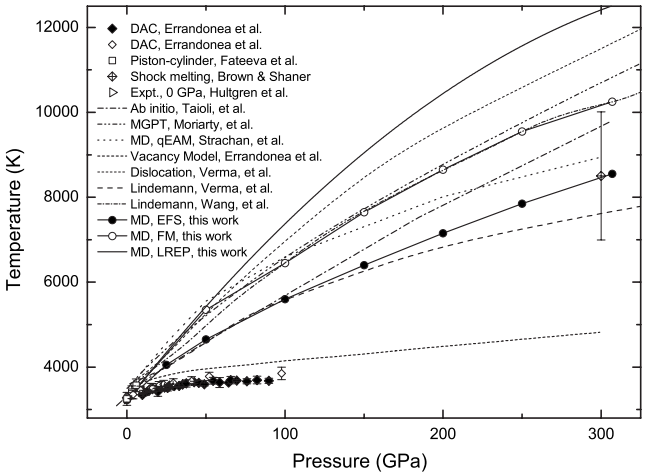

FIG. 8. Calculated melting curves with the three types of potentials in comparison with DAC experiments (Refs. 4, 5, and 7), 0 GPa values (Ref. 51), piston-cylinder results (Ref. 1), shock melting temperature (Ref. 2), and calculations (Refs. 8, 11, 12, 15, 24, and 25).

It is known that the shock meting pressure (as well as solid-solid phase transitions) was inferred from the abrupt decrease of acoustic velocity with the increasing shock compressions, whereas the melting temperature was only deduced from the thermodynamic models based upon some assumptions for the specific heat, the Grüneisen parameter, etc. Under the shock heat rate of 10^{12} K/s, Ta remains superheated before melting and has the superheating rate of 0.23,[52] so superheating corrections are necessary for the reported shock melting temperature.[25,52] From the superheating rate of 0.23, we deduced the shock melting temperature for Ta is 6910 K. For DAC melting curve, it has a slope of nearly zero and the melting temperature extrapolated to 300 GPa is about 4800 K,[25] in contrast with the original

TABLE III. Melting temperatures of Ta from EFS potential at various pressures.

P (GPa)	T_m (K)
0	3225±25
25	4050±50
50	4650±50
100	5600±10
150	6400±10
200	7150±50
250	7850±50
307	8550±50

shock melting temperature of 8500±1500 K,[2] and present calculation results of 8550±50 K. Apparently, there is still a large discrepancy between the DAC extrapolations and inferred shock melting temperature near 300 GPa, even though the superheating corrections are considered.

All the theoretical calculations including present results indicate that the disagreements with DAC results are very large. At the very low pressure region, theoretical results support the DAC data, whereas in the pressure range of around 10–100 GPa the disagreements with DAC increase dramatically. Calculations based on molecular dynamics, ab initio quantum mechanics and results from the empirical melting models (including Lindemann law, phenomenological vacancy model, and dislocation melting model) mainly offer the supports for the shock temperature, however, the vacancy melting curve of Errandonea *et al.*[25] tend to support the DAC experiments. Nevertheless, the results of different theoretical methods differ largely especially in high pressure region, and these various theoretical methods have their own advantages and disadvantages. As for classical molecular dynamics, it can treat extremely large systems but the used potential function should be tested carefully to be valid in high pressure region according to equation of state, thermal expansion, and so on, otherwise, the errors cannot be eliminated properly (for instance, the comparison of present three melting curves). *Ab initio* quantum mechanical simulations are widely accepted as the most accurate approach to a very wide range of physical properties of materials. However, the empirical models are based mainly upon the phenomenological laws, and the different models have the very large differences in melting curves of Ta.[12,24,25] It was reported recently that the dislocation melting model can give large differences for the melting temperatures of transition metal such as Ta if the starting parameters are slightly modified.[6] The Lindemann law is also an empirical law based on earlier experimental investigations of simple gases at low pressure, whereas it may be questioned when it is used to calculate the melting properties of transition metals under extremely high temperatures and pressures.[5,53] Hence, all the theoretical methods have their own limitations to describe the high pressure properties of materials, but each one cast a description or explanation on melting properties of Ta from different aspect.

It was shown that solid-liquid transitions begin with nucleation, in which the Gibbs free energy barrier to the formation of a nucleus of the daughter phase should be overcome.[54] While, in two-phase method, there is no difficulty in nucleating either the liquid or solid phases, as the interface assists in the nucleation for the melting or crystallization process.[26] So in one-phase method, the considerable superheating may be included in the results.[52,55,56] However, for present molecular dynamics simulations, we applied two-phase (coexistence) method and the nucleation-induced superheating is automatically eliminated from the simulations with two solid-liquid interfaces.[26] While, we treated Ta as "ideal" solid and liquid in our simulations, this probably overestimated the melting temperature to some extent, because we did not take into account the possible existence of local structures (packing of fivefold symmetric icosahedral clusters), whose free energy is lower than that of ideal liquid.[57] And similarly the local structures with fivefold symmetry are also observed in the stable liquid which strengthen upon supercooling through *ab initio* molecular dynamics by Jakse *et al.* in Ta, as well as with other symmetries in supercooled liquid Zr and Ni.[58–60]

In melting experiments such as DAC and shock wave, the surfaces play a crucial role in the melting transition; that is, to maintain pressure, the sample surface must be acted upon by some pressure-transmitting medium. Sorkin *et al.*[61] indicated that the differences observed between DAC and SW experiments are in the fact that: the shock melting resembles a mechanical lattice instability due to the presence of a rigid medium, however, in DAC experiments the presence of a soft medium at the sample surface boundary will cause melting to begin at a lower temperature, being better described by thermodynamics theories. The restriction of the out-of-plane motion by the rigid medium in SW experiments suppresses thermal disordering of the surface, so superheating is possible.[61] And in the SW experiments the free surface was eliminated to be closer to an infinite solid, as is similar to the molecular dynamics simulations with three-dimensional periodic boundary conditions. Hence, according to the theory of Sorkin *et al.*, present MD results also include surface-induced superheating in them.

The melting temperature is largely affected by the vacancy formation energy, which is a measure of the strength of nearest-neighbor bonds that need to be broken to form the vacancy. The higher vacancy formation energy a metal have, the higher melting temperature it can reach. The strong directional bonds arising from the incomplete d-shells give rise to high vacancy formation energies and also give rise to high melting temperature in transition metals like Ta.[62,63] It is reported that interpreting melting in terms of the generation of vacancies indeed provide a plausible explanation for the melting curve measured in DAC experiments and its low slope.[5,62,63]

The DAC techniques used to experimentally determine the melting curve of tantalum provided the best estimates for the melting curve of Ta.[14] In addition, the same techniques have been used to study the melting curve of other metals such as alkaline-earth metals,[64] Cu, and Ni (Ref. 65) and some of the results obtained have been confirmed by *ab initio* calculations.[66,67] However, the large discrepancy between the extrapolated DAC results and the superheating corrected shock melting temperature still exists, so the possible reasons can naturally be attributed to either the existence of new phases in both solid and liquid Ta under high pressures and high temperatures or the differences of melting mechanism between DAC and shock wave experiments. But the problem nowadays remains unsolved and present meting curve is just one of the predictions from molecular dynamics for the melting of tantalum. Therefore, more experimental measurements are urgently necessary to further determine the phases and then the whole melting curve of tantalum. Apart from extending DAC experiments to higher pressure region, the improved shock techniques are also good choices, such as the measurement technique of Tan *et al.*[68]

IV. CONCLUSION

In conclusion, we have performed the coexistence phase molecular dynamics with three types of potentials to obtain

the melting curve of Ta at 0–307 GPa. Through a series of tests, we have found that the EFS potential is the reliable potential for simulating both solid and liquid Ta. The EFS potential also produced the satisfying melting curve, which accords well with experiments at low pressures and accords well with shock melting at high pressures. The other two curves of LREP and FM potentials have no the satisfying agreement with shocking melting at high pressures. So, we believe the EFS potential is the reliable potential for simulating both solid and liquid Ta under high pressures and high temperatures. The large discrepancy between the extrapolated DAC results and the superheating corrected shock melting temperature still exists, so more experimental measurements are urgently necessary to further determine the phases and then the whole melting curve of tantalum.

ACKNOWLEDGMENTS

The authors would like to thank D. Alfè for helpful discussions. We also acknowledge the support by the National Natural Science Foundation of China under Grant No. 10776029/A06 and the NSAF under Grant No. 10776022.

*Corresponding author: xrchen@scu.edu.cn

[1] N. S. Fateeva and L. F. Vereshchagin, Sov. Phys. JETP **16**, 322 (1971).
[2] J. M. Brown and J. W. Shaner, *Shock Waves in Condensed Matter* (Elsevier, New York, 1984).
[3] R. S. Hixson, D. A. Boness, J. W. Shaner, and J. A. Moriarty, Phys. Rev. Lett. **62**, 637 (1989).
[4] D. Errandonea, B. Schwager, R. Ditz, C. Gessmann, R. Boehler, and M. Ross, Phys. Rev. B **63**, 132104 (2001).
[5] D. Errandonea, M. Somayazulu, D. H. Usermann, and H. K. Mao, J. Phys.: Condens. Matter **15**, 7635 (2003).
[6] D. Errandonea, J. Phys.: Condens. Matter **16**, 8801 (2004).
[7] D. Errandonea, J. Phys. Chem. Solids **67**, 2018 (2006).
[8] J. A. Moriarty, J. F. Belak, R. E. Rudd, P. Soderlind, F. H. Streitz, and L. H. Yang, J. Phys.: Condens. Matter **14**, 2825 (2002).
[9] S. N. Luo, T. J. Ahrens, T. Cagin, A. Strachan, W. A. Goddard, and D. C. Swift, Phys. Rev. B **68**, 134206 (2003).
[10] A. B. Belonoshko, S. I. Simak, A. E. Kochetov, B. Johansson, L. Burakovsky, and D. L. Preston, Phys. Rev. Lett. **92**, 195701 (2004).
[11] A. Strachan, T. Cagin, O. G. lseren, S. Mukherjee, R. E. Cohen, and W. A. G. III, Modell. Simul. Mater. Sci. Eng. **12**, S445 (2004).
[12] A. K. Verma, R. S. Rao, and B. K. Godwal, J. Phys.: Condens. Matter **16**, 4799 (2004).
[13] C. Cazorla, M. J. Gillan, S. Taioli, and D. Alfè, J. Chem. Phys. **126**, 194502 (2007).
[14] S. N. Luo and D. C. Swift, Physica B **388**, 139 (2007).
[15] S. Taioli, C. Cazorla, M. J. Gillan, and D. Alfè, Phys. Rev. B **75**, 214103 (2007).
[16] L. M. Hsiung and D. H. Lassila, Scr. Mater. **38**, 1371 (1998).
[17] L. M. Hsiung and D. H. Lassila, Scr. Mater. **39**, 603 (1998).
[18] N. C. Holmes, J. A. Moriarty, G. R. Gathers, and W. J. Nellis, J. Appl. Phys. **66**, 2962 (1989).
[19] A. C. Mitchell and W. J. Nellis, J. Appl. Phys. **52**, 3363 (1981).
[20] W. J. Nellis, A. C. Mitchell, and D. A. Young, J. Appl. Phys. **93**, 304 (2003).
[21] J. A. Moriarty, Phys. Rev. B **49**, 12431 (1994).
[22] P. Soderlind and J. A. Moriarty, Phys. Rev. B **57**, 10340 (1998).
[23] H. Cynn and C. S. Yoo, Phys. Rev. B **59**, 8526 (1999).
[24] Y. Wang, R. Ahuja, and B. Johansson, Phys. Rev. B **65**, 014104 (2001).
[25] D. Errandonea, Physica B **357**, 356 (2005).
[26] J. R. Morris, C. Z. Wang, K. M. Ho, and C. T. Chan, Phys. Rev. B **49**, 3109 (1994).
[27] M. J. Gillan, D. Alfè, J. Brodholt, L. Vocadlo, and G. D. Price, Rep. Prog. Phys. **69**, 2365 (2006).
[28] J. R. Morris and X. Song, J. Chem. Phys. **116**, 9352 (2002).
[29] T. Ogitsu, E. Schwegler, F. Gygi, and G. Galli, Phys. Rev. Lett. **91**, 175502 (2003).
[30] A. B. Belonoshko and L. S. Dubrovinsky, Am. Mineral. **81**, 303 (1996).
[31] K. Harfuji, T. Tsuchiya, and K. Kawamura, J. Appl. Phys. **96**, 2501 (2004).
[32] A. B. Belonoshko, R. Ahuja, and B. Johansson, Phys. Rev. Lett. **84**, 3638 (2000).
[33] X. D. Dai, Y. Kong, J. H. Li, and B. X. Liu, J. Phys.: Condens. Matter **18**, 4527 (2006).
[34] X. D. Dai, J. H. Li, and Y. Kong, Phys. Rev. B **75**, 052102 (2007).
[35] F. Ercolessi and J. B. Adams, Europhys. Lett. **26**, 583 (1994).
[36] Y. H. Li, D. J. Siegel, J. B. Adams, and X. Y. Liu, Phys. Rev. B **67**, 125101 (2003).
[37] The potential can be obtained at http://enpub.fulton.asu.edu/cms/potentials/main/main.htm
[38] J. P. Perdew, K. Burke, and M. Ernzerhof, Phys. Rev. Lett. **77**, 3865 (1996).
[39] S. Y. Savrasov, Phys. Rev. B **54**, 16470 (1996).
[40] O. K. Andersen, Phys. Rev. B **12**, 3060 (1975).
[41] A. Dewaele, P. Loubeyre, and M. Mezouar, Phys. Rev. B **70**, 094112 (2004).
[42] W. Smith, T. R. Forester, I. T. Todorov, and M. Leslie, *The DL POLY_2 user manual*, CCLRC Daresbury Laboratory Daresbury, Warrington WA4 4AD Cheshire, UK, Version 2.17, December 2006.
[43] H. J. C. Berendsen, J. P. M. Postma, W. v. Gunsteren, A. DiNola, and J. R. Haak, J. Chem. Phys. **81**, 3684 (1984).
[44] U. Essmann, L. Perera, M. L. Berkowitz, T. Darden, H. Lee, and L. G. Pedersen, J. Chem. Phys. **103**, 8577 (1995).
[45] D. Alfè, M. J. Gillan, and G. D. Price, J. Chem. Phys. **116**, 6170 (2002).
[46] J. W. Edwards, R. Speiser, and H. L. Johnston, J. Appl. Phys. **22**, 424 (1951).
[47] H. Jager, W. Neff, and G. Pottlacher, Int. J. Thermophys. **13**, 83 (1992).
[48] S. P. Marsh, *Los Alamos Shock Hugoniot Data* (University of California Press, Berkeley, 1979.
[49] Y. Wang, D. Q. Chen, and X. W. Zhang, Phys. Rev. Lett. **84**,

3220 (2000).
[50] D. Orlikowski, P. Söderlind, and J. A. Moriarty, Phys. Rev. B **74**, 054109 (2006).
[51] R. Hultgren, P. D. Desai, D. T. Hawkins, M. Gleiser, K. K. Kelley, and D. D. Wagman, *Selected Values of the Thermodynamical Properties of the Elements* (American Society for Metals, Metals Park, OH, 1973).
[52] S. N. Luo and T. J. Ahrens, Appl. Phys. Lett. **82**, 1836 (2003).
[53] C. Dai, H. Tan, and H. Geng, J. Appl. Phys. **92**, 5019 (2002).
[54] S. N. Luo, A. Strachan, and D. C. Swift, J. Chem. Phys. **120**, 11640 (2004).
[55] Z. H. Jin and K. Lu, Philos. Mag. Lett. **78**, 29 (1998).
[56] S. N. Luo, J. L. Mosenfelder, P. D. Asimow, and T. J. Ahrens, Phys. Usp. **40**, 435 (2002).
[57] M. Ross, R. Boehler, and S. Japel, J. Phys. Chem. Solids **67**, 2178 (2006).
[58] N. Jakse, O. L. LeBacq, and A. Pasturel, Phys. Rev. B **70**, 174203 (2004).
[59] N. Jakse and A. Pasturel, Phys. Rev. Lett. **91**, 195501 (2003).
[60] N. Jakse and A. Pasturel, J. Chem. Phys. **120**, 6124 (2004).
[61] V. Sorkin, E. Polturak, and J. Adler, Europhys. Lett. **76**, 623 (2006).
[62] S. Mukherjee, R. E. Cohen, and O. Gülseren, J. Phys.: Condens. Matter **15**, 885 (2003).
[63] C. C. Matthai and N. H. March, Philos. Mag. Lett. **87**, 475 (2007).
[64] D. Errandonea, R. Boehler, and M. Ross, Phys. Rev. B **65**, 012108 (2001).
[65] S. Japel, B. Schwager, R. Boehler, and M. Ross, Phys. Rev. Lett. **95**, 167801 (2005).
[66] L. Vočadlo, D. Alfè, G. D. Price, and M. J. Gillan, J. Chem. Phys. **120**, 2872 (2004).
[67] S. Mehta, G. D. Price, and D. Alfè, J. Chem. Phys. **125**, 194507 (2006).
[68] H. Tan, C. D. Dai, L. Y. Zhang, and C. H. Xu, Appl. Phys. Lett. **87**, 221905 (2005).